Original Article

Comparative study of physiological FDG uptake in small structures between silicon photomultiplier-based PET and conventional PET

Running title: SiPM vs. conventional PET in FDG

Shiro Watanabe[1,2], Kenji Hirata[1,2,3], Keiichi Magota[4], Junki Takenaka[1,2], Naoto Wakabayashi[1,2], Daiki Shinyama[5], Koichi Yasuda[6], Akihiro Homma[7], Kohsuke Kudo[1,3,8]

1. Department of Diagnostic Imaging, Hokkaido University Graduate School of Medicine, Kita 15 Nishi 7, Kita-ku, Sapporo, Hokkaido, 060-8638, Japan.

2. Department of Nuclear Medicine, Hokkaido University Hospital, Kita 14 Nishi 5, Kita-ku, Sapporo, Hokkaido, 060-8648, Japan.

3. Division of Medical AI Education and Research, Hokkaido University Graduate School of Medicine, Sapporo, Japan.

4. Division of Medical Imaging and Technology, Hokkaido University Hospital, Sapporo, Japan.

5. Philips Japan, Ltd., Tokyo, Japan.

6. Department of Radiation Oncology, Hokkaido University Hospital, Sapporo, Japan.

7. Department of Otolaryngology-Head and Neck Surgery, Faculty of Medicine and Graduate School of Medicine, Hokkaido University, Sapporo, Japan.

8. Global Center for Biomedical Science and Engineering, Faculty of Medicine, Hokkaido University, Sapporo, Japan.

Corresponding author:

Kenji HIRATA, MD, PhD, FANMB, FJCR

Department of Diagnostic Imaging, Graduate School of Medicine, Hokkaido University

Kita 15, Nishi 7, Kita-Ku, Sapporo, Hokkaido, Japan 060-8638

Phone: 81-11-706-7779 Fax: 81-11-706-7408 email: khirata@med.hokudai.ac.jp

Sources of funding: This study was partially supported by grants from the Japan Society for the Promotion of Science (JSPS) KAKENHI (no. 20K16781) and Japan's MEXT KAKENHI (no. 18K18412).

Conflicts of interest: Daiki Shinyama was an employee of Philips Japan, Ltd. The other authors declare no conflicts of interest in regard to this manuscript.

ABSTRACT

Objective: Silicon photomultiplier-based positron emission tomography/computed tomography (SiPM-PET/CT) has superior spatial resolution to conventional PET/CT (cPET/CT). This head-to-head comparison study compared the images of physiological 18F-fluorodeoxyglucose (FDG) accumulation in small-volume structures between SiPM-PET/CT and cPET/CT in patients scanned with both modalities, and we investigated whether the thresholds that are reported to be useful for differentiating physiological accumulations from malignant lesions can also be applied to SiPM-PET/CT.

Methods: We enrolled 21 consecutive patients with head and neck malignancies who underwent whole-body FDG-PET/CT for initial staging or a follow-up evaluation (October 2020 to March 2022). After being injected with FDG, all patients underwent PET acquisition on both Vereos PET-CT and Gemini TF64 PET-CT systems (both Philips Healthcare) in random order. For each patient, the maximum standardized uptake value (SUVmax) was measured in the pituitary gland, esophagogastric junction (EGJ), adrenal glands, lumbar enlargement of the spinal cord, and epididymis. We measured the liver SUVmean and the blood pool SUVmean to calculate the target-to-liver ratio (TLR) and the target-to-blood ratio (TBR), respectively. Between-group differences in each variable were examined by a paired t-test. We also investigated whether there were cases of target uptake greater than the reported threshold for distinguishing pathological from physiological

accumulations.

Results: Data were available for 19 patients. Ten patients were in Group 1, i.e., the patients who underwent SiPM-PET first, and the remaining nine patients who underwent cPET first were Group 2. In the SiPM-PET results, the SUVmax of all targets was significantly higher than that obtained by cPET in all patients, and this tendency was also observed when the patients were divided into Groups 1/2. The TLRs of all targets were significantly higher in SiPM-PET than in cPET in all patients, and SiPM-PET also showed significantly higher TBRs for all targets except the EGJ ($p=0.052$).

Conclusions: The physiological uptake in the small structures studied herein showed high accumulation on SiPM-PET. Our results also suggest that the thresholds reported for cPET to distinguish pathological accumulations likely lead to false-positive findings in SIPM-PET evaluations.

Key words: silicon photomultiplier, PET/CT, SUVmax, 18F-FDG

Introduction

Fully digital positron emission tomography (PET) cameras such as that used in the Vereos system (Philips, Cleveland, OH, USA) feature small digital silicon photomultipliers (SiPMs) instead of much larger photomultiplier tubes, providing true digital photon counting with 1-to-1 crystal coupling [1]. Compared to conventional PET/computed tomography (cPET/CT), SiPM-PET/CT allows for more accurate quantifications and characterizations of patients with cancer, due to its improved spatial resolution, system sensitivity, and image contrast [2–6]. The Philips Vereos has a spatial resolution of 4.2 mm as the full width at half-maximum (FWHM) and a dramatic enhancement in time-of-flight (TOF) resolution compared to Gemini TF PET (Philips) systems [7].

The improved performance of SiPM-PET/CT has enhanced the ability to detect lesions <1 cm in size in patients with malignant tumors [8–10], and thus even areas showing physiologic accumulation may be seen as hyperaccumulation in structures with a small volume, i.e., ≤1 cm. In patients with malignancies plus multiple metastases, such accumulations may be misidentified as metastatic lesions, and the degree of accumulation needs to be identified. In addition, many of the indices that have been reported to be useful for differentiating physiological accumulations from malignant lesions were obtained with the use of cPET, and we speculated that these values are unlikely to be readily applicable to SiPM-PET/CT.

We conducted the present study to: (*i*) compare the imaging of physiological FDG

accumulations in small-volume structures of cancer patients scanned with both SiPM-PET/CT and cPET, and (*ii*) determine whether the thresholds reported as useful for differentiating physiological accumulations from malignant lesions are also applicable for use with SiPM-PET/CT.

Patients and Methods

This study was a retrospective analysis of data obtained in a prospective study approved by the Ethical Review Committee of our institution (#020-0170). The requirement for patients' written informed consent was waived. Twenty-one consecutive patients with head and neck malignancies who underwent whole-body FDG PET/CT for initial staging or a follow-up evaluation between October 2020 and March 2022 at our institution were included in the study.

FDG-PET/CT acquisition and reconstruction

All patients fasted for ≥6 hours prior to PET/CT scanning. The PET images were acquired with both a Vereos PET-CT and a Gemini TF64 PET-CT system (Philips Healthcare, Cleveland, OH) in random order. After the patient underwent blood glucose testing indicating the absence of hyperglycemia, and 60 minutes after a single injection of 4.5 MBq/kg FDG, he or she underwent imaging on the first scanner and then on the second scanner (Fig. 1); more details about the interval between scans is provided below. During these scans, the patient's head was held by a headrest to

restrict head motions. The scans were acquired during mid-expiration. No oral or intravenous contrast agent was administered.

For the patients' Gemini TF examinations, the parameters for the CT were 120 kVp, pitch of 0.671, 30 mAs, and 4-mm slice thickness. For the PET scanning, the matrix size was 144 × 144; the voxel size was 4.0 × 4.0 × 4.0 mm. The scan time per bed position was 2.0 min/bed. Images were reconstructed using the blob-based ordered subset expectation maximization (OSEM) algorithm reinforced with the TOF algorithm. Point-spread-function (PSF) correction was not applied.

For the patients' Vereos examinations, the parameters for the CT were 120 kVp, pitch of 0.828, 26 mAs, and 2-mm slice thickness. For the PET scanning, the matrix size was 288 × 288; the voxel size was 2.0 × 2.0 × 2.0 mm. The scan time per bed position was 2.0 min/bed. Images were reconstructed using the blob-based OSEM algorithm. Both the TOF algorithm and PSF correction were applied.

FDG PET/CT analysis

The 21 patients' PET/CT data were evaluated by the same board-certified nuclear medicine physician (S.W.). All PET scans were first visually analyzed using a standardized uptake value (SUV) readout scale of 0–4 g/mL in Metavol software [11]. For each patient, the maximum standardized uptake value (SUVmax) was measured in the pituitary gland, esophagogastric junction (EGJ),

adrenal glands, lumbar enlargement of the spinal cord (LE), and epididymis. A spherical volume of interest (VOI) with a 3-cm diameter was set in the right lobe of the liver as a reference region to calculate the liver SUVmean, and a spherical 5-mm-dia. VOI was set in the descending aorta; the blood pool SUVmean was calculated. The target-to-liver ratio (TLR) was calculated by dividing the target SUVmax by the liver SUVmean. The target-to-blood ratio (TBR) was calculated by dividing the target SUVmax by the blood pool SUVmean.

Patients' head MRI and upper gastrointestinal endoscopy performed within the 6 months prior to the PET examinations, if available, confirmed structural abnormalities in the pituitary gland and EGJ. Bilateral adrenal and LE and bilateral epididymis were confirmed by CT for attenuation-correction findings of structural abnormalities.

We also investigated whether there were cases of target uptake that was greater than the reported thresholds for distinguishing pathological from physiological accumulations shown. The threshold values of SUV were set at 4.1 for the pituitary [12], SUVmax 5.2 for adrenal glands [13], 5.0 for testis [14], and 3.5 for EGJ [15]. Since there was no corresponding report of an SUV threshold for the epididymis, we used reports concerning the testis instead. We were also unable to examine LE thresholds because we could not find any reports concerning an LE threshold.

Statistical analysis

All values are expressed as the mean ± standard deviation. We divided the patients into two groups according to the order of PET/CT imaging; in Group 1, the SiPM-PET/CT was performed first and in Group 2, the cPET/CT was performed first. All data were analyzed with JMP® Version 16.0 software (SAS Institute Inc., Cary, NC, 1989–2023). Each variable between the two groups was compared by a paired t-test. The level of significance was $p \leq 0.05$.

Results

Of the total of 21 patients, two patients could not continue the examination with the second scanner due to severe cough and severe neck pain, respectively, and SiPM-PET data were not obtained; data were thus available for 19 patients. The patients' characteristics are summarized in Table 1. There were 15 males (78.9%) and 4 females (21.1%) aged 61.7 ± 11.8 years. The purpose of FDG PET/CT imaging was initial staging in 12 patients (63.2%) and follow-up evaluation in 7 patients (36.8%). Ten patients (52.6%) were in Group 1, i.e., they underwent scanning with SiPM-PET first, and the remaining nine patients (47.4%) were in Group 2, in which cPET scanning was performed first. After FDG administration, the first scan was performed at 59.9 ± 2.8 min and the second scan was performed at 105.4 ± 4.1 min. The mean time delay between the two scans was 45.5 ± 3.3 min.

Brain MRI had been performed within the prior 6 months in 13 of the 19 patients (68.4%), and

no structural abnormality of the pituitary gland was noted in any patient. Upper endoscopy was performed in 15 of the 19 patients (78.9%): gastroesophageal reflex disease was identified in seven patients (46.7%), and stage 0 esophageal cancer at the lower thoracic region was detected in one patient (6.7%). Adrenocortical nodular hyperplasia and adrenocortical adenoma were each observed in a single patient (5.3%). There was no CT abnormality in the LE of the spinal cord or bilateral epididymis.

Quantitative analysis

In the patients' SiPM-PET results, the SUVmax was significantly higher than that obtained with cPET in any targets in the entire patient series (Fig. 2). This tendency was also observed when the patients were divided into Groups 1 and 2 (Table 2).

The comparison of the liver and blood pool SUVmean values between the SiPM-PET and cPET in all patients revealed no significant difference. However, in the analysis of the patients divided into Group 1 and Group 2, the SUVmean was significantly higher in the first scanner in both groups (Table 2).

The TLRs obtained by SiPM-PET were significantly higher than those obtained by cPET in all of the targets in all patient groups (Fig. 3a). The TBRs from SiPM-PET were also significantly higher for all targets except the EGJ ($p=0.052$) (Fig. 3b). In Group 1, the pituitary, adrenal, and LE

TLRs were significantly higher in SiPM-PET, whereas the epididymis TBR was significantly higher in cPET. In Group 2, in contrast, the TLRs and TBRs of all targets were significantly higher on SiPM-PET (Tables 3, 4).

Reevaluation of the reported threshold

The pituitary of five patients (26.3%) showed an SUVmax above the reported threshold in their SiPM-PET results (four patients underwent SiPM-PET as their 1st scan, and the other did so as the 2nd scan), whereas the cPET results of all of the patients showed an SUVmax above the reported threshold. There were no cases of accumulation in the adrenal gland that exceeded the threshold SUVmax 5.2. In six patients (40.0%), the epididymis accumulation exceeded the threshold in the imaging by SiPM-PET (one patient as the 1st scan and five in the 2nd scan). Accumulation in the EJG exceeded the threshold in four (21.1%) patients' SiPM-PET images (all four: 2nd scan) and in one (5.3%) patient's cPET images too (1st scan). The images of representative patients are presented in Figures 4 and 5.

Discussion

All of the physiological accumulation sites in the small-volume structures examined herein showed high FDG accumulation in SiPM-PET images. This was true not only for the SUVmax but

also for the TBR and TLR, and it was independent of the order of the patients' SiPM-PET and cPET examinations. Our results also suggest that the cPET thresholds that have been reported for distinguishing pathological accumulations are likely to result in false positives when adapted for evaluations of SiPM-PET images.

Our observation of higher accumulations shown by SiPM-PET in the evaluations of lesion accumulations based on imaging modalities provided by various vendors is generally consistent with previous reports [3,6,9,16–20]. Factors that determine the SUV include hardware differences (e.g., the field-of-view length and TOF performance) and software differences (e.g., the image reconstruction method, PSF availability, matrix size, and uptake and acquisition times). In particular, the spatial resolution (4.0 mm for the Vereos PET-CT and 4.8 mm for the Gemini TF64 PET-CT) and the temporal resolution at TOF (322 ps for Vereos PET-CT and 502 ps for Gemini TF64 PET-CT) are superior in the Vereos PET-CT system used herein compared to the Gemini TF64 PET-CT system, resulting in an improved signal-to-noise ratio (SNR) and improved contrast [7].

López-Mora et al. evaluated 22 patients and reported that the lesions that were not detected by analog PET/CT but were detected by digital PET/CT were all <10 mm [9]. Since the lesions that we examined in the present study are all small in structure, we speculate that our results involve the same mechanism as that involved in the earlier reports that small lymph node metastases and distant metastases can be detected more frequently on SiPM-PET. As SiPM-PET continues to become more

commonly used, we should be aware that physiologic hyperaccumulations may be observed, unlike the cPET accumulations identified previously.

In the present series of patients, there was a significant difference in the SUVmax for each target between the two systems, whether SiPM-PET or cPET was performed first. This may be because the uptake into the structures studied herein was essentially physiological glucose metabolism, with little effect of delayed uptake. The SUVmean values in the mediastinal blood pool and liver were not significantly different between the two systems but was lower in the patients' second scanner. This may be ascribed to a temporal decrease in vascular activity due to the continuous clearance of FDG by the kidneys [3]. Importantly, the quantification performance of the Vereos PET-CT and Gemini TF64 PET-CT systems was comparable, and thus the TBRs and TLRs were also higher on SiPM-PET with its improved spatial resolution, but the cPET images when performed as the second PET examination may present TLRs and TBRs that are similar to those obtained by SiPM-PET due to the reduced uptake of FDG into the blood pool and liver.

The above discussion indicates that the SUVmax, TLR, and TBR are high in evaluations using SiPM-PET. It should be noted that when obtained in routine practice, these values are higher in the new SiPM-PET imaging of patients who have been previously imaged with cPET. In addition, the thresholds that have been reported to be useful for distinguishing benign and malignant states are based on cPET and produced false positives in up to 40% of our study population. In the pituitary

gland, because benign tumors of pituitary adenomas are also hyperaccumulated, tumorigenic and inflammatory changes as well as stress have been proposed as thresholds for hyperaccumulation, i.e., an SUV ≥5.0 [12]. However, in the present SiPM PET examinations, the results for five patients (26.3%) were false positive despite being nonpathological. Evaluations that derive the SUV, TLR, and/or TBR should be considered, as there is a high overlap between physiological and pathological uptakes, and the presence of organic abnormalities should also be evaluated with multimodality.

Study limitations are as follows. The number of patients was small (n=19); however, statistically significant differences in the patients' data were identified. In addition, not all of the patients were adequately investigated for organic lesions. Our study included head and neck malignancies, and the intensity of physiologic accumulation may be different in healthy subjects. In the two sets of PET images compared in this study, the reconstruction method differed with and without PSF or the matrix size, but this was due to the vendor's default settings in both systems. Other conditions were kept the same as much as possible, but differences in the SUV may be due to these reconstruction methods as well as differences in the equipment. One may argue that the different matrix sizes of reconstructed images might have caused the different SUVmax measured. However, when 2mm was selected as the voxel size for the Gemini TF64 PET-CT, post-reconstruction smoothing must be needed due to poor SNR. In contrast, the Vereos PET-CT has better SNR than the TF due to its improved TOF performance, which allows image reconstruction with 2mm voxel. The

present comparison of FDG evaluation between the systems under optimized clinical conditions may be valuable.

In conclusion, the physiological uptake in the small-volume structures analyzed herein showed high accumulation in SiPM-PET. The results also suggest that the thresholds reported for cPET to distinguish pathological accumulations are likely to lead to false-positive findings in SIPM-PET evaluations. It is important to note that accumulations on SiPM-PET can appear pathological if not interpreted with care, especially in patients with carcinoma.

Reference

1. Frach T, Prescher G, Degenhardt C, de Gruyter R, Schmitz A, Ballizany R. The digital silicon photomultiplier — Principle of operation and intrinsic detector performance. 2009 IEEE Nucl Sci Symp Conf Rec NSSMIC. 2009. p. 1959–65.

2. Delcroix O, Bourhis D, Keromnes N, Robin P, Le Roux P-Y, Abgral R, et al. Assessment of Image Quality and Lesion Detectability With Digital PET/CT System. Front Med. 2021;8:629096.

3. Fuentes-Ocampo F, López-Mora DA, Flotats A, Paillahueque G, Camacho V, Duch J, et al. Digital vs. analog PET/CT: intra-subject comparison of the SUVmax in target lesions and reference regions. Eur J Nucl Med Mol Imaging. 2019;46:1745–50.

4. Van Der Vos CS, Koopman D, Rijnsdorp S, Arends AJ, Boellaard R, Van Dalen JA, et al. Quantification, improvement, and harmonization of small lesion detection with state-of-the-art PET. Eur J Nucl Med Mol Imaging. 2017;44:4–16.

5. Kojima I, Takanami K, Ogawa T, Sakamoto M, Nagai H, Miyashita H, et al. High detection sensitivity and reliable morphological correlation of PET with a silicon photomultiplier for primary tongue squamous cell carcinoma. Ann Nucl Med. 2020;34:643–52.

6. Kim SH, Song B-I, Kim HW, Won KS. Comparison of Image Quality and Semi-quantitative Measurements with Digital PET/CT and Standard PET/CT from Different Vendors. Nucl Med Mol Imaging. 2020;54:233–40.

7. Zhang J, Maniawski P, Knopp MV. Performance evaluation of the next generation solid-state digital photon counting PET/CT system. EJNMMI Res. 2018;8:97.

8. Oddstig J, Leide Svegborn S, Almquist H, Bitzén U, Garpered S, Hedeer F, et al. Comparison of conventional and Si-photomultiplier-based PET systems for image quality and diagnostic performance. BMC Med Imaging. 2019;19:81.

9. López-Mora DA, Flotats A, Fuentes-Ocampo F, Camacho V, Fernández A, Ruiz A, et al. Comparison of image quality and lesion detection between digital and analog PET/CT. Eur J Nucl

Med Mol Imaging. 2019;46:1383–90.

10. Miwa K, Wagatsuma K, Nemoto R, Masubuchi M, Kamitaka Y, Yamao T, et al. Detection of sub-centimeter lesions using digital TOF-PET/CT system combined with Bayesian penalized likelihood reconstruction algorithm. Ann Nucl Med. 2020;34:762–71.

11. Hirata K, Kobayashi K, Wong K-P, Manabe O, Surmak A, Tamaki N, et al. A semi-automated technique determining the liver standardized uptake value reference for tumor delineation in FDG PET-CT. PloS One. 2014;9:e105682.

12. Hyun SH, Choi JY, Lee K-H, Choe YS, Kim B-T. Incidental focal 18F-FDG uptake in the pituitary gland: clinical significance and differential diagnostic criteria. J Nucl Med Off Publ Soc Nucl Med. 2011;52:547–50.

13. Kunikowska J, Matyskiel R, Toutounchi S, Grabowska-Derlatka L, Koperski L, Królicki L. What parameters from 18F-FDG PET/CT are useful in evaluation of adrenal lesions? Eur J Nucl Med Mol Imaging. 2014;41:2273–80.

14. Higgins A, Kim H, Harper L, Habermann TM, Nowakowski GS, Thompson CA, et al. Testicular FDG-PET/CT uptake threshold in aggressive lymphomas. Am J Hematol. 2021;96:E81–3.

15. Stagg J, Farukhi I, Lazaga F, Thompson C, Bradshaw L, Kaif M, et al. Significance of 18F-

Fluorodeoxyglucose Uptake at the Gastroesophageal Junction: Comparison of PET to Esophagogastroduodenoscopy. Dig Dis Sci. 2015;60:1335–42.

16. van Sluis J, Boellaard R, Somasundaram A, van Snick PH, Borra RJH, Dierckx RAJO, et al. Image Quality and Semiquantitative Measurements on the Biograph Vision PET/CT System: Initial Experiences and Comparison with the Biograph mCT. J Nucl Med Off Publ Soc Nucl Med. 2020;61:129–35.

17. Wagatsuma K, Sakata M, Ishibashi K, Hirayama A, Kawakami H, Miwa K, et al. Direct comparison of brain [18F]FDG images acquired by SiPM-based and PMT-based PET/CT: phantom and clinical studies. EJNMMI Phys. 2020;7:70.

18. Tsutsui Y, Awamoto S, Himuro K, Kato T, Baba S, Sasaki M. Evaluating and comparing the image quality and quantification accuracy of SiPM-PET/CT and PMT-PET/CT. Ann Nucl Med. 2020;34:725–35.

19. de Jong TL, Koopman D, van Dalen JA, Tegelaar A, van Dijk JD, Stevens H, et al. Performance of digital PET/CT compared with conventional PET/CT in oncologic patients: a prospective comparison study. Ann Nucl Med. 2022;36:756–64.

20. Zimmermann P-A, Houdu B, Césaire L, Nakouri I, De Pontville M, Lasnon C, et al. Revisiting

detection of in-transit metastases in melanoma patients using digital 18F-FDG PET/CT with small-voxel reconstruction. Ann Nucl Med. 2021;35:669–79.

Figure Legends

Fig. 1. The FDG-PET/CT protocol performed on the two PET systems (Vereos and Gemini TF).

Fig. 2. The distribution of maximum standardized uptake (SUVmax) values in the target structures measured by the two PET systems. EGJ: esophagogastric junction.

Fig. 3. Comparison of **(a)** the target-to-liver ratio (TLR) and **(b)** the target-to-blood ratio (TBR) with SiPM PET and cPET in small structures.

Fig. 4. Typical images of the pituitary gland. SiPM PET images at the pituitary level **(a)**, PET-CT fusion images **(b)**, PET images on cPET **(c)**, and PET-CT fusion images **(d)**. This patient was first scanned with SiPM-PET, which showed an accumulation with SUVmax 4.69, TLR 1.57, and TBR 3.15 on SiPM PET, and SUVmax 2.91, TLR 1.04, and TBR 3.18 on cPET in the pituitary gland. The SiPM PET images showed more nodular and clear accumulation.

Fig. 5. Typical images of lumbar enlargement (LE) of the spinal cord. Spinal cord-level sagittal CT image **(a)**, SiPM PET image **(b)**, and cPET image **(c)**. The patient was first scanned by cPET, which

showed an accumulation with SUVmax 3.80, TLR 1.83, and TBR 3.06 on SiPM PET and SUVmax 2.02, TLR 0.82, and TBR 1.14 on cPET in the LE of the spinal cord. The SiPM PET image showed more nodular and clear accumulation.

Acknowledgements

We thank Ronee Asad (Philips Japan, Tokyo) and Piotr J. Maniawski (Philips Healthcare, Cleveland, OH, USA) for their great support.

Table 1. Characteristics of the 19 patients with head/neck malignancies whose data were complete

No.	Sex	Age, yrs	FDG, MBq/kg	Type of cancer	PET order	1st scan	2nd scan
1	M	56	4.33	Cancer of unknown primary	Group 1	58	94
2	M	56	4.47	Hypopharyngeal cancer	Group 2	60	106
3	M	70	4.45	Hypopharyngeal cancer	Group 1	60	106
4	F	22	4.61	Submandibular adenocarcinoma	Group 2	61	105
5	M	75	4.58	Nasopharyngeal cancer	Group 1	59	111
6	M	62	4.47	Oropharyngeal cancer	Group 2	60	107
7	M	67	4.46	Hypopharyngeal cancer	Group 1	58	102
8	M	70	4.41	Maxillary sinus cancer	Group 1	59	111
9	M	69	4.37	Oropharyngeal cancer	Group 2	62	107
10	F	61	4.44	Thyroid cancer	Group 1	63	107
11	F	65	4.21	Maxillary sinus cancer	Group 2	67	110
12	M	77	4.48	Tongue cancer	Group 1	56	101
13	F	54	4.63	Oropharyngeal cancer	Group 2	60	104
14	M	56	4.31	Hypopharyngeal cancer	Group 2	58	107
15	M	59	4.42	Laryngeal cancer	Group 1	57	101
16	M	55	4.39	Nasopharyngeal cancer	Group 1	58	104
17	M	75	4.24	Nasopharyngeal cancer	Group 1	65	110
18	M	66	4.35	Nasopharyngeal cancer	Group 2	61	108
19	M	57	4.32	Nasopharyngeal cancer	Group 2	56	101

Group 1: SiPM PET/CT performed first, Group 2: cPET/CT performed first.

Table 2. Comparison of SUVs with SiPM PET and cPET in small structure uptake

Location	Scanner order	SiPM PET	cPET	p-value
Pituitary	Group 1	3.82 ± 1.07	2.62 ± 0.53	0.001
	Group 2	3.51 ± 0.91	2.50 ± 0.51	0.004
Adrenal glands	Group 1	2.93 ± 0.70	2.18 ± 0.43	<0.001
	Group 2	3.19 ± 0.75	2.15 ± 0.27	<0.001
Lumbar enlargement of the spine cord	Group 1	2.94 ± 0.58	2.18 ± 0.31	<0.001
	Group 2	3.37 ± 0.48	1.99 ± 0.14	<0.001
Epididymis	Group 1	4.08 ± 0.76	3.29 ± 0.55	<0.001
	Group 2	5.32 ± 0.70	2.86 ± 0.21	<0.001
Esophagogastric junction	Group 1	3.01 ± 0.35	2.36 ± 0.34	<0.001
	Group 2	3.85 ± 1.94	2.57 ± 0.72	0.030
Liver, SUVmean	Group 1	2.65 ± 0.33	2.30 ± 0.36	<0.001
	Group 2	2.07 ± 0.28	2.45 ± 0.26	<0.001
Blood pool, SUVmean	Group 1	1.55 ± 0.16	1.15 ± 0.18	<0.001
	Group 2	1.09 ± 0.14	1.46 ± 0.17	0.001

Data are mean ± standard deviation (SD). Group 1: SiPM PET/CT performed first, Group 2: cPET/CT performed first. cPET: conventional PET, SiPM PET: silicon photomultiplier-based PET, SUV: standardized uptake value, SUVmean: mean standardized uptake value.

Table 3. Comparison of the target-to-liver ratio (TLR) with SiPM PET/CT and cPET/CT in small structure uptake

Location	Scanner order	SiPM PET	cPET	p-value
Pituitary	Group 1	1.44 ± 0.36	1.15 ± 0.22	0.008
	Group 2	1.68 ± 0.28	1.02 ± 0.15	<0.001
Adrenal gland	Group 1	1.11 ± 0.22	0.96 ± 0.17	<0.001
	Group 2	1.54 ± 0.25	0.89 ± 0.14	<0.001
Lumbar enlargement of the spine cord	Group 1	1.11 ± 0.17	0.97 ± 0.19	0.039
	Group 2	1.64 ± 0.24	0.82 ± 0.12	<0.001
Epididymis	Group 1	1.56 ± 0.23	1.46 ± 0.23	0.146
	Group 2	2.46 ± 0.42	1.11 ± 0.09	<0.001
Esophagogastric junction	Group 1	1.15 ± 0.23	1.05 ± 0.20	0.054
	Group 2	1.84 ± 0.80	1.05 ± 0.26	0.007

Data are mean ± SD. Group 1: SiPM PET/CT performed first, Group 2: cPET/CT performed first. cPET: conventional PET, SiPM PET: silicon photomultiplier-based PET.

Table 4. Comparison of the target-to-blood ratio (TBR) with SiPM PET/CT and cPET/CT in small structure uptake

Location	Scanner order	SiPM PET	cPET	p-value
Pituitary	Group 1	2.45 ± 0.59	2.32 ± 0.51	0.39
	Group 2	3.27 ± 0.86	1.74 ± 0.42	<0.001
Adrenal gland	Group 1	1.88 ± 0.37	1.93 ± 0.43	0.588
	Group 2	2.99 ± 0.83	1.49 ± 0.22	<0.001
Lumbar enlargement of the spine cord	Group 1	1.91 ± 0.41	1.97 ± 0.54	0.589
	Group 2	3.17 ± 0.69	1.38 ± 0.20	<0.001
Epididymis	Group 1	2.67 ± 0.37	2.95 ± 0.57	0.039
	Group 2	5.05 ± 0.99	1.96 ± 0.17	0.002
Esophagogastric junction	Group 1	1.96 ± 0.32	2.10 ± 0.38	0.231
	Group 2	3.73 ± 2.37	1.78 ± 0.53	0.023

Data are mean ± SD. Group 1: SiPM PET/CT performed first, Group 2: cPET/CT performed first. cPET: conventional PET, SiPM PET: silicon photomultiplier-based PET.

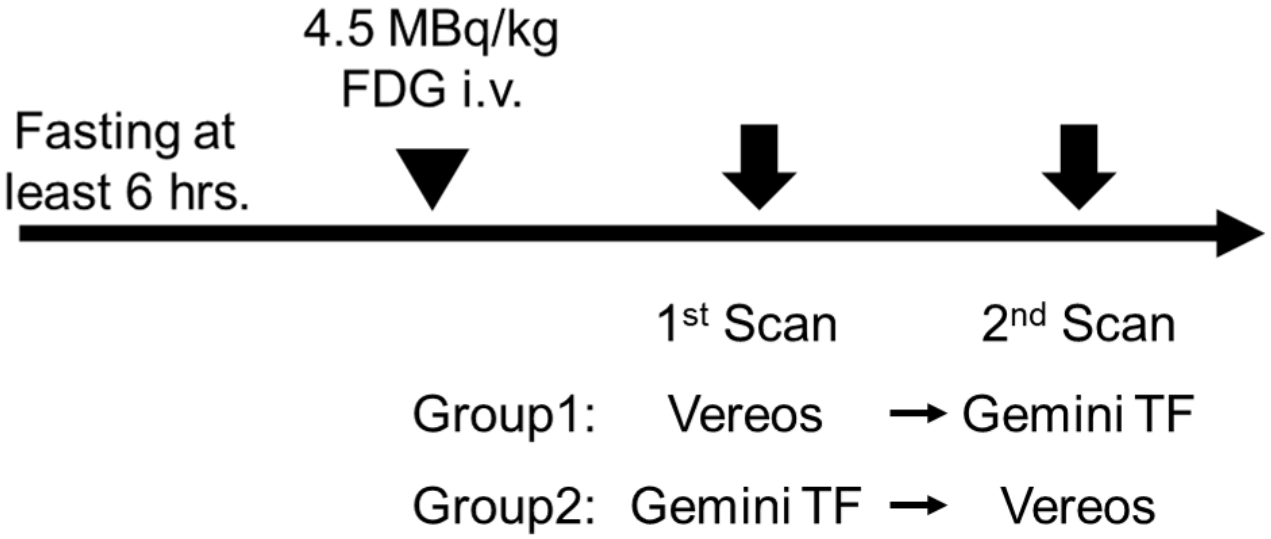
4.5 MBq/kg
FDG i.v.
Fasting at
least 6 hrs.
1st Scan
2nd Scan
Group1: Vereos → Gemini TF
Group2: Gemini TF → Vereos

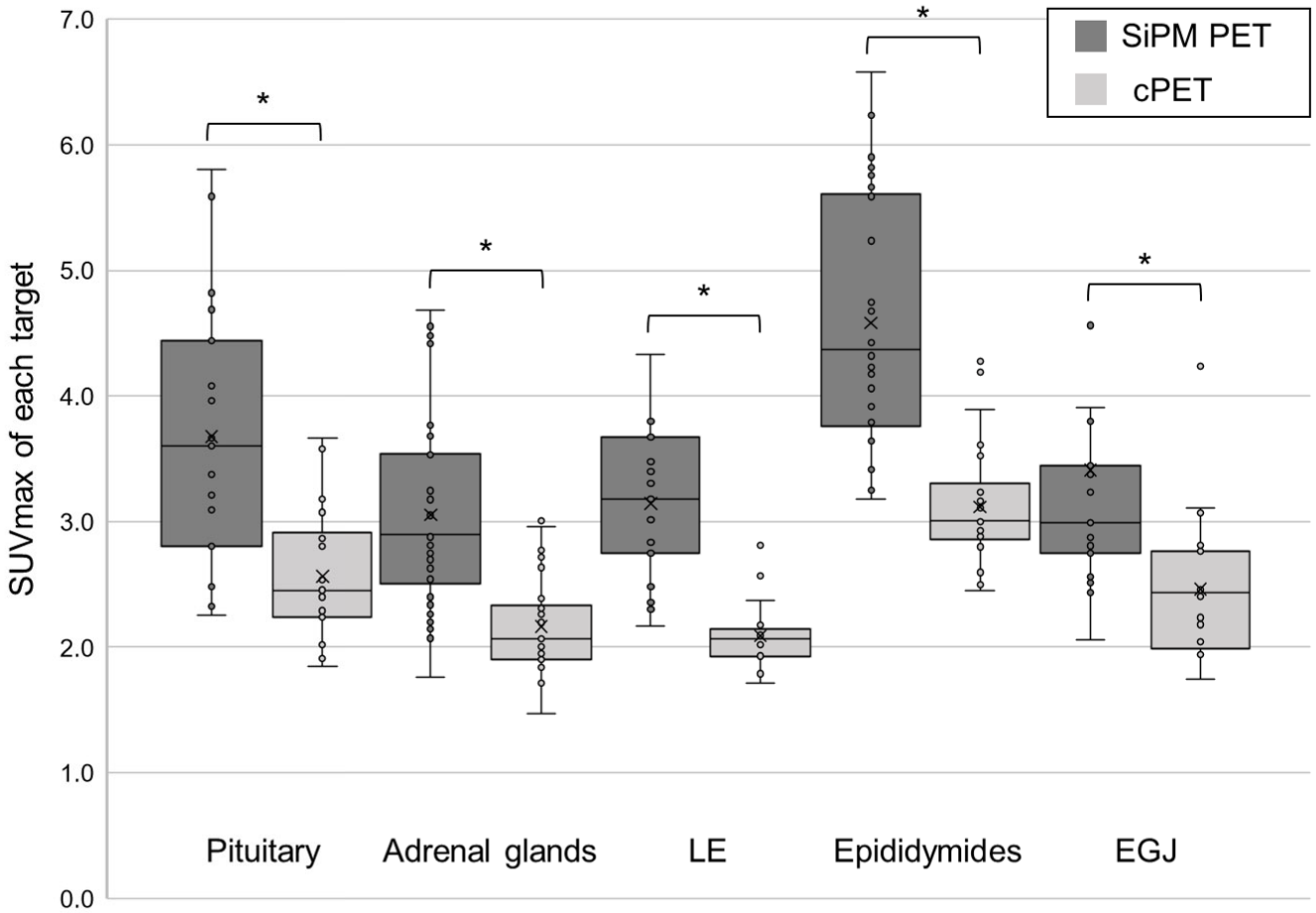
SiPM PET
cPET
SUVmax of each target
7.0
6.0
5.0
4.0
3.0
2.0
1.0
0.0
*
*
*
*
*
Pituitary
Adrenal glands
LE
Epididymides
EGJ

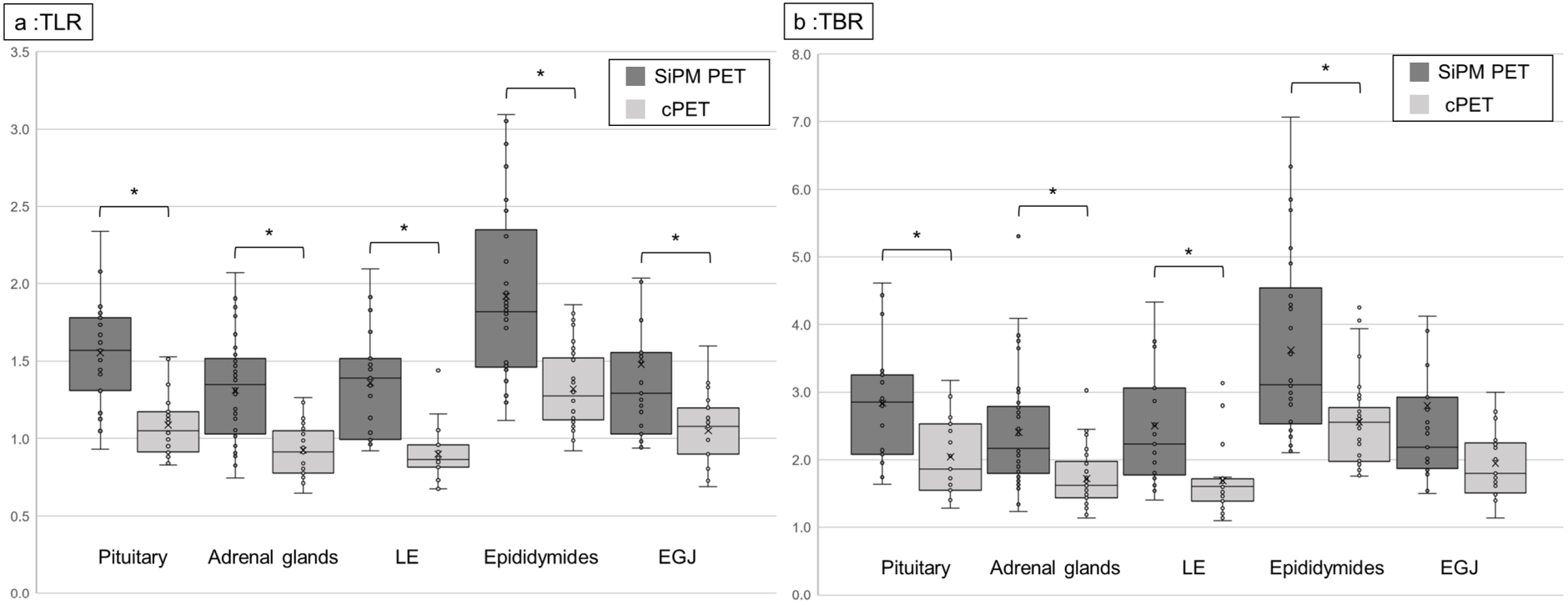
a :TLR
SiPM PET
cPET
3.5
3.0
2.5
2.0
1.5
1.0
0.5
0.0
*
Pituitary
Adrenal glands
LE
Epididymides
EGJ
b :TBR
SiPM PET
cPET
8.0
7.0
6.0
5.0
4.0
3.0
2.0
1.0
0.0
*
Pituitary
Adrenal glands
LE
Epididymides
EGJ

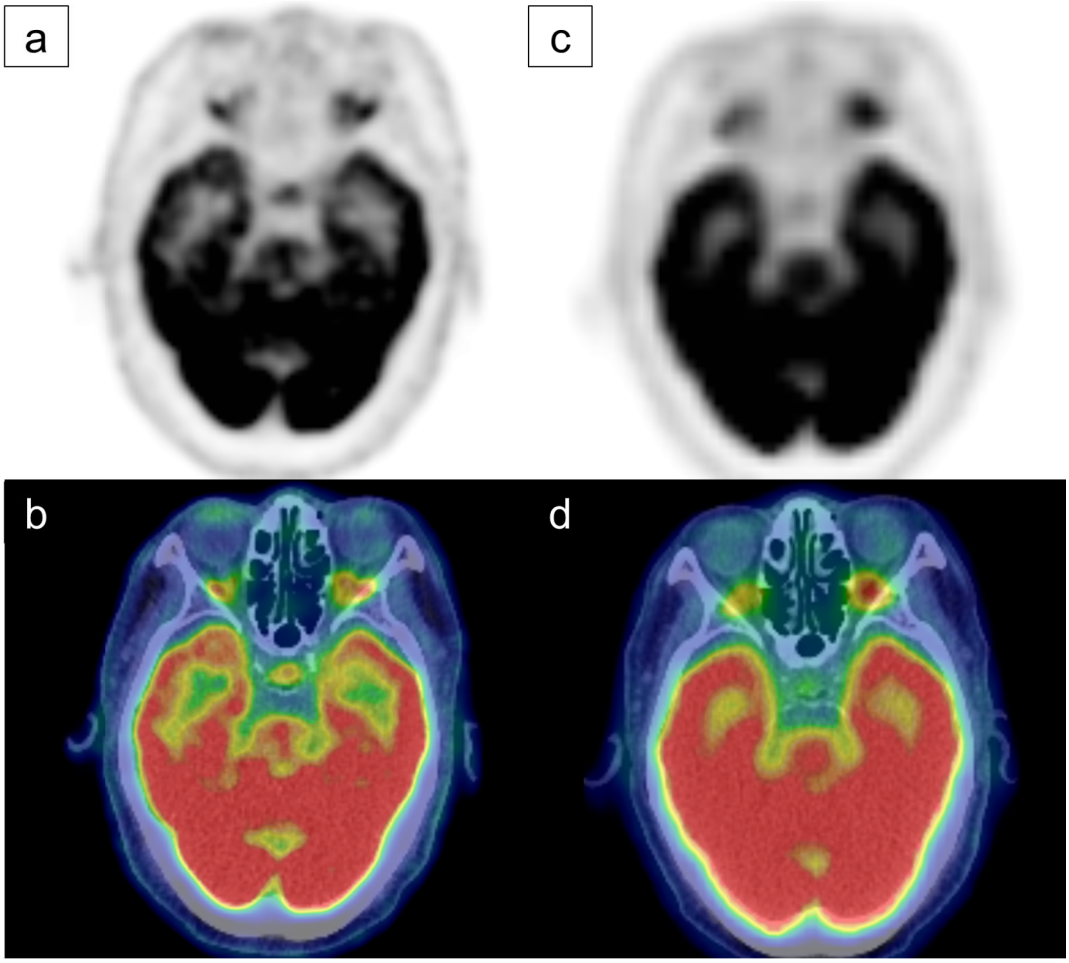
a
c
b
d

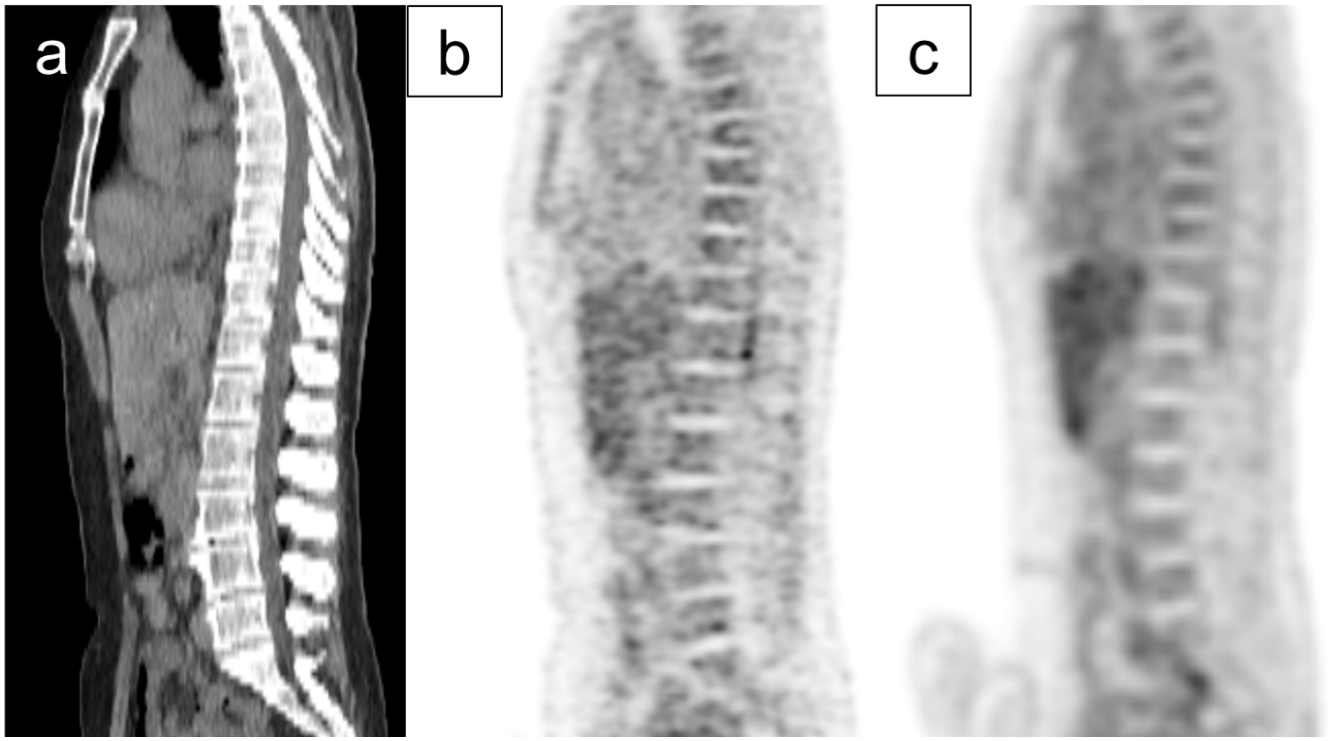
a
b
c